Geophysical Research Letters

RESEARCH LETTER
10.1029/2020GL089435

Lower Crustal Rheology Controls the Development of Large Offset Strike-Slip Faults During the Himalayan-Tibetan Orogeny

Jianfeng Yang[1,2,3], Boris J. P. Kaus[2], Yang Li[1], Philippe Hervé Leloup[4], Anton A. Popov[2], Gang Lu[1], Kun Wang[1], and Liang Zhao[1]

[1]State Key Laboratory of Lithospheric Evolution, Institute of Geology and Geophysics, Chinese Academy of Sciences, Beijing, China, [2]Institute of Geosciences, Johannes Gutenberg University Mainz, Mainz, Germany, [3]Dipartimento di Geoscienze, Università di Padova, Padova, Italy, [4]Laboratoire de Géologie de Lyon, Université de Lyon 1, ENS de Lyon, CNRS, UMR 5276 LGL-TPE, Villeurbanne, France

Abstract The mechanism of crustal deformation and the development of large offset strike-slip faults during continental collision, such as the India-Eurasia zone, remains poorly understood. Previous mechanical models were simplified which are either (quasi-)2-D approximations or made the a priori assumption that the rheology of the lithosphere was either purely viscous (distributed deformation) or purely localized. Here we present three-dimensional visco-elasto-plastic thermo-mechanical simulations, which can produce both distributed and highly localized deformation, to investigate crustal deformation during continental indentation. Our results show that large-scale shear zones develop as a result of frictional plasticity, which have many similarities with observed shear zones. Yet localized deformation requires both a strong upper crust (>10^{22} Pa·s) and a moderately weak middle/lower crust (~10^{20} Pa·s) in Tibet. The brittle shear zones in our models develop low viscosity zones directly beneath them, consistent with geological observations of exhumed faults, and geophysical observations across active faults.

Plain Language Summary Large offset strike-slip faults are one of the key surface features of continental collision, such as in Tibet. These narrow belts of strike-slip faults accommodate strong deformation, and deciphering their mechanism of formation helps to understand the complex dynamics of India-Eurasia collision. Yet previous models developed to address this either assumed simplified rheologies or employed low numerical resolutions that is insufficient to simulate the spontaneous formation of localized zones. Here, we present high-resolution 3-D visco-elasto-plastic thermo-mechanical models that simulate the formation of large-scale strike-slip faults during Indian indentation, while also taking distributed deformation into account. Our simulations show that a combination of a strong upper crust and a moderately weak middle/lower crust produces faults that are, to first order, consistent with observed ones in the Tibet region. Localized deformation usually initiates at the brittle-ductile transition, and a weak middle/lower crust facilitates subsequent shear localization such that the shear zones cut through the whole crust. The craton-like strong terranes can sustain large stresses and initiate large offset faults along their boundaries.

Key Points:
- 3D VEP high-resolution thermomechanical models accounting for both localized and distributed deformation during India-Eurasia collision
- Major strike-slip faults develop preferentially in models with a strong upper and a moderately weak lower crust
- Lower crustal flow and strong terranes surrounding Tibet facilitate fault formation

Supporting Information:
- Supporting Information S1

Correspondence to:
L. Zhao,
zhaoliang@mail.iggcas.ac.cn

Citation:
Yang, J., Kaus, B. J. P., Li, Y., Leloup, P. H., Popov, A. A., Lu, G., et al. (2020). Lower crustal rheology controls the development of large offset strike-slip faults during the Himalayan-Tibetan orogeny. *Geophysical Research Letters*, *47*, e2020GL089435. https://doi.org/10.1029/2020GL089435

Received 26 JUN 2020
Accepted 4 SEP 2020

1. Introduction

The Himalayan-Tibetan orogen is a spectacular example of continent-continent collision, which resulted in pervasive crustal deformation in Asia (Yin & Harrison, 2000). Such deformation includes several large-scale, extending 1,000 km long, strike-slip faults (Figure 1) that developed through the collision history (Molnar & Tapponnier, 1975; Tapponnier et al., 1986). The mechanisms of fault development and the partitioning of crustal deformation, however, are poorly understood. Several endmember models have been proposed for lithospheric deformation in Tibet and surrounding regions, including an extrusion model suggesting that deformation is primarily localized along large-scale strike-slip faults and thrust zones (Replumaz & Tapponnier, 2003; Tapponnier et al., 1982, 2001); thin viscous sheet models suggesting that shortening is distributed and vertically coherent within the lithosphere (England & McKenzie, 1982; Houseman & England, 1986); and channel flow models implying that a thickened weak channel develops in the lower crust which spreads the deformation front outward from the plateau (Clark & Royden, 2000; Royden et al., 1997).

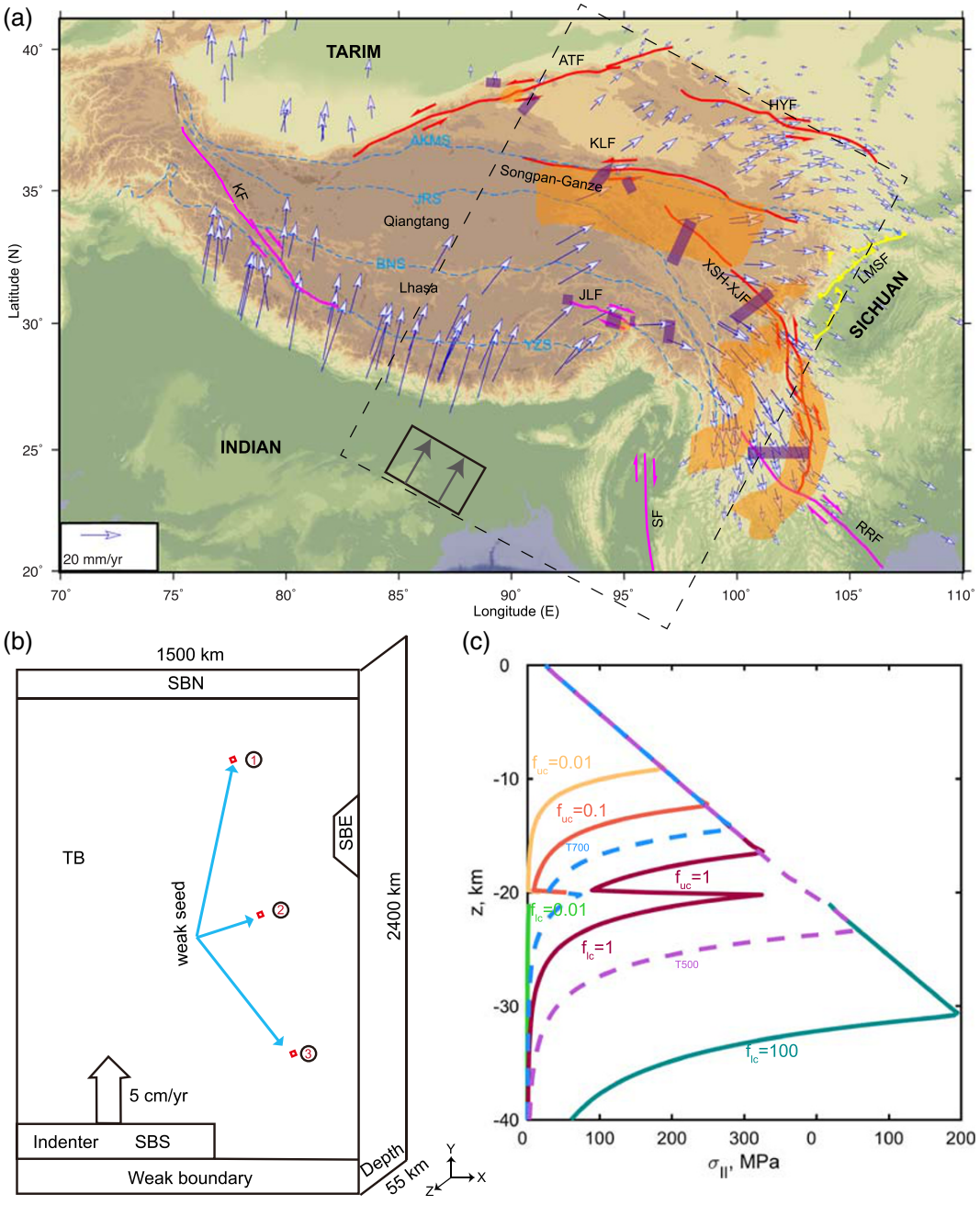

Figure 1. (a) Geological map in Tibet and surrounding region. Blue arrows are GPS data from Gan et al. (2007); orange shaded regions are low seismic velocity zones (Bao et al., 2015; Li et al., 2014; Liu et al., 2014; Wittlinger et al., 1998); purple shaded regions are high electrical conductivity zones (Bai et al., 2010; Dong et al., 2016; Le Pape et al., 2012; Wei et al., 2014; Zhang et al., 2015). The black dashed zone is roughly our model region. The cyan dashed lines correspond to main suture zones: YZS = Yalung-Zangpo suture; BNS = Bangong-Nujiang suture; JRS = Jinsha River suture; AKMS = Anyimaqen-Kunlun-Muztagh suture. Active faults are as follows: SF = Sagaing Fault; RRF = Red River Fault; XSH-XJF = Xianshuihe-Xiaojiang Fault; KLF = Kunlun Fault; HYF = Haiyuan Fault; ATF = Altyn-Tagh Fault; KF = Karakorum Fault. (b) Schematic model setup. The indenter is pushed with 5 cm/yr; three weak seeds (numbered) are preset as shown by red square. The locations of the weak seeds (10 km × 10 km × 10 km) are at depth of 10 km and (950 km, 1,950 km), (1,050 km, 1,150 km), and (1,250 km, 550 km) in *x-y* plane, respectively. Three strong blocks (SBs) in the north (SBN), south (SBS), and east (SBE), respectively, are added as well. (c) Upper/lower crust strength for our models for a constantly imposed extensional background strain rate of 10^{-15} s^{-1}.

Deformation style varies from normal faulting to thrust and strike-slip faulting across the plateau and its periphery, indicating complex deformation processes during the India-Eurasia collision. Present-day strain partitioning is locally mainly localized along major strike-slip faults, supporting an extrusion model (Li et al., 2018). Geophysical studies show that at several locations low seismic velocity zones are coincident at depth with high electrical conductivity zones around the large offset strike-slip faults (Agius & Lebedev, 2014; Bai et al., 2010; Baumann & Kaus, 2015; Nelson et al., 1996; Wu et al., 2019) (Figure 1). These anomalous zones in the middle-lower crust are generally attributed to high temperature, the presence of aqueous fluids, and/or partial melting (Li et al., 2020; Liu & Hasterok, 2016), which will all significantly weaken the crustal strength (Kaus, 2016; Liu & Hasterok, 2016) beneath the faults. Furthermore, the present-day deformation mode in the lower crust remains a matter of debate: Copley et al. (2011) argue in favor of a strong lower crust beneath Tibet to explain strike-slip faulting in the north and normal faulting in the south, which contrasts with the channel flow model (e.g., Clark & Royden, 2000). As geophysical data give a snapshot of present-day crustal and mantle structures, the properties before collision remain unclear, and its role in the evolution of plateau growth and crustal deformation remains ambiguous.

The development of crustal deformation and topography are strongly dependent on the rheology of the crust, which is the fundamental distinction among the endmember models listed above. Nevertheless, most previous models were either fully plastic for the block model or fully viscous for thin sheet and lower crustal flow models. Recent numerical models mostly focus on the development of topography (Chen et al., 2017; Lechmann et al., 2011; Pusok & Kaus, 2015) and subduction dynamics (Capitanio, 2020; Li et al., 2013; Replumaz et al., 2016; Sternai et al., 2014), emphasizing the effect of variable lateral and vertical lithosphere strength across multiple terranes (Bischoff & Flesch, 2018; Chen et al., 2017; Huangfu et al., 2018). Such models provide valuable insights in the dynamics of the lithospheric deformation, but the limited resolution of these models inhibits resolving strongly localized deformation within the crust in a three-dimensional (3-D) framework.

Here, we employ high-resolution three-dimensional thermo-mechanical numerical models to investigate the role of crustal rheology on the formation of large strike-slip fault during the indentation of India into Asia.

2. Model Description

We employ the 3-D parallel thermo-mechanical numerical code LaMEM (Kaus et al., 2016), which is based on a finite difference staggered grid discretization combined with a particle-in-cell technique using a conservative velocity interpolation approach (Pusok et al., 2017). It solves the energy, momentum, and mass conservation using a geometric multigrid approach (see supporting information for detail). Our simulations are performed for a 1,500 km × 2,400 km × 55 km (Figure 1) region (using 512 × 768 × 32 cells) and employ a simplified tectonic structure with nonlinear visco-elasto-plastic rheologies (Pusok et al., 2018; Wang et al., 2019), designed to investigate crustal deformation of an India-like indenter into Asia. The 40-km-thick crust is composed of a 20-km upper and a 20-km-thick lower crust in Tibetan Block (TB) region, respectively. The vertical grid resolution has been increased to 1.25 km in the upper crust to capture localized deformation (Duretz et al., 2020). The mechanical boundary conditions are free slip for all boundaries, but to mimic a free surface condition in finite difference scheme, we use a 15-km "sticky-air" layer as well as with a free surface stabilization algorithm (Crameri et al., 2012; Kaus et al., 2010). The strong indenter collides with a constant convergence (5 cm/yr) into TB (Figure 1). Three weak seeds are placed in the TB region (the effect of their locations is tested, as described below). For simplicity, we employ an initial linear temperature profile with a fixed temperature of 0°C at the surface and 600°C at the bottom, while other boundaries have zero thermal flux.

The rheology of rocks (Table S1) is assumed to be visco-elasto-plastic, and the total deviatoric strain rate is given by

$$\dot{\varepsilon}_{ij} = \dot{\varepsilon}_{ij}^{vis} + \dot{\varepsilon}_{ij}^{el} + \dot{\varepsilon}_{ij}^{pl} = \frac{1}{2\eta_{eff}}\tau_{ij} + \frac{1}{2G}\frac{D\tau_{ij}}{Dt} + \dot{\lambda}\frac{\partial Q}{\partial \sigma_{ij}} \quad (1)$$

where $\dot{\varepsilon}_{ij}^{vis}$, $\dot{\varepsilon}_{ij}^{el}$, $\dot{\varepsilon}_{ij}^{pl}$ denote viscous, elastic, and plastic strain rate, respectively. η_{eff} is the effective viscosity, G elastic shear modulus, t time, $\dot{\lambda}$ plastic multiplier, Q plastic flow potential, and $\sigma_{ij} = -P+\tau_{ij}$ the total stress. The power law viscosity is given by

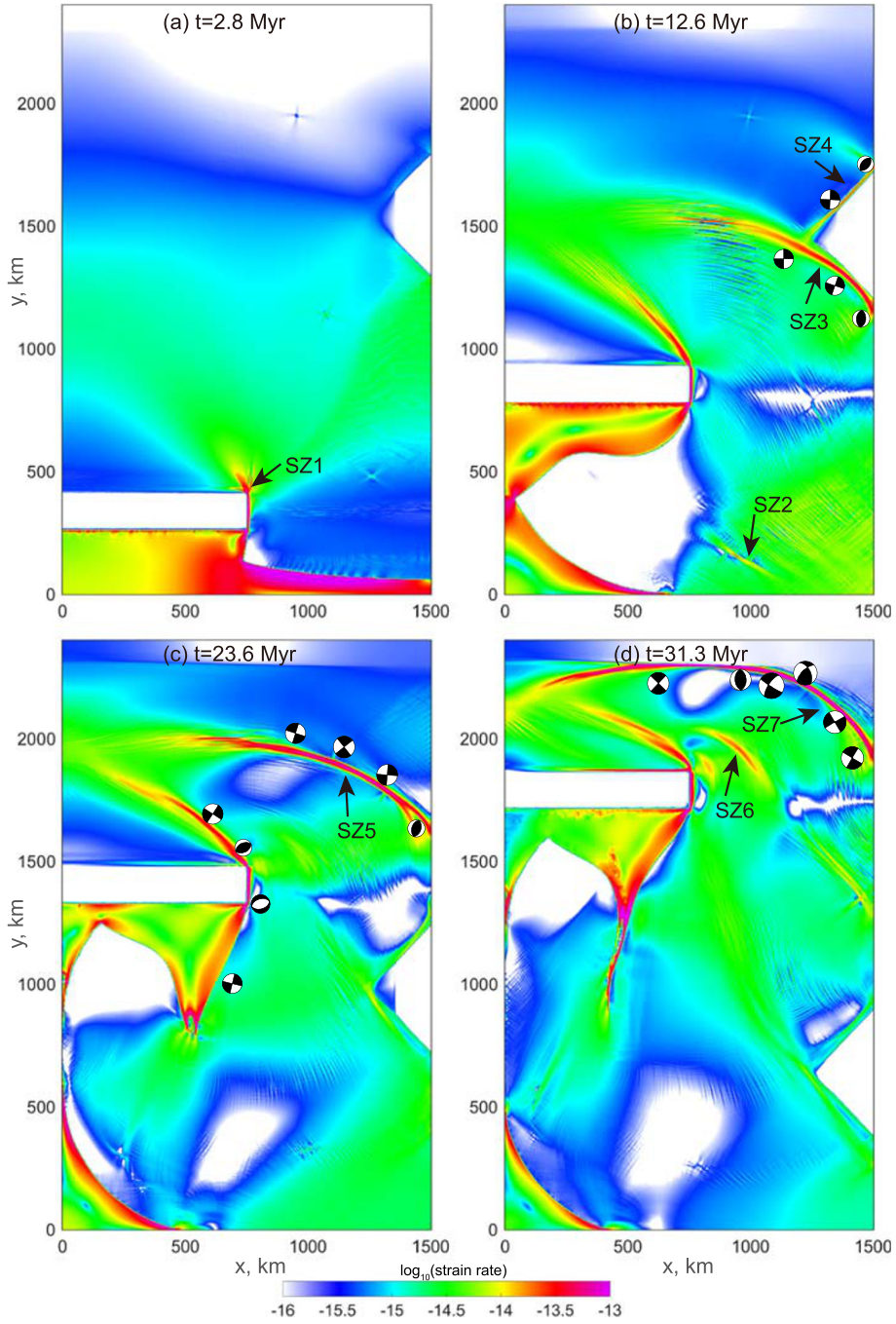

Figure 2. Second invariant of the total strain rate tensor at 10-km depth at four representative time stages. The arrows indicate seven large-scale shear zones (SZ). These shear zones are strike-slip faults, while locally show reverse and normal faults as shown in the beachballs (see the supporting information for detail).

$$\eta_{eff} = \frac{1}{2} f B_N^{-1/n} \exp\left(\frac{E + PV}{nRT}\right) \dot{\varepsilon}_{II}^{\frac{1}{n}-1} \tag{2}$$

where f is the scaling factor used in the simulations (Lu et al., 2016), B_N is the prefactor, n is the stress exponent of dislocation creep, $\dot{\varepsilon}_{II} = \sqrt{0.5 \dot{\varepsilon}_{ij}^{vis} \dot{\varepsilon}_{ij}^{vis}}$ is the second invariant of the viscous strain rate tensor, E, V are activation energy and activation volume, respectively, and R is the gas constant.

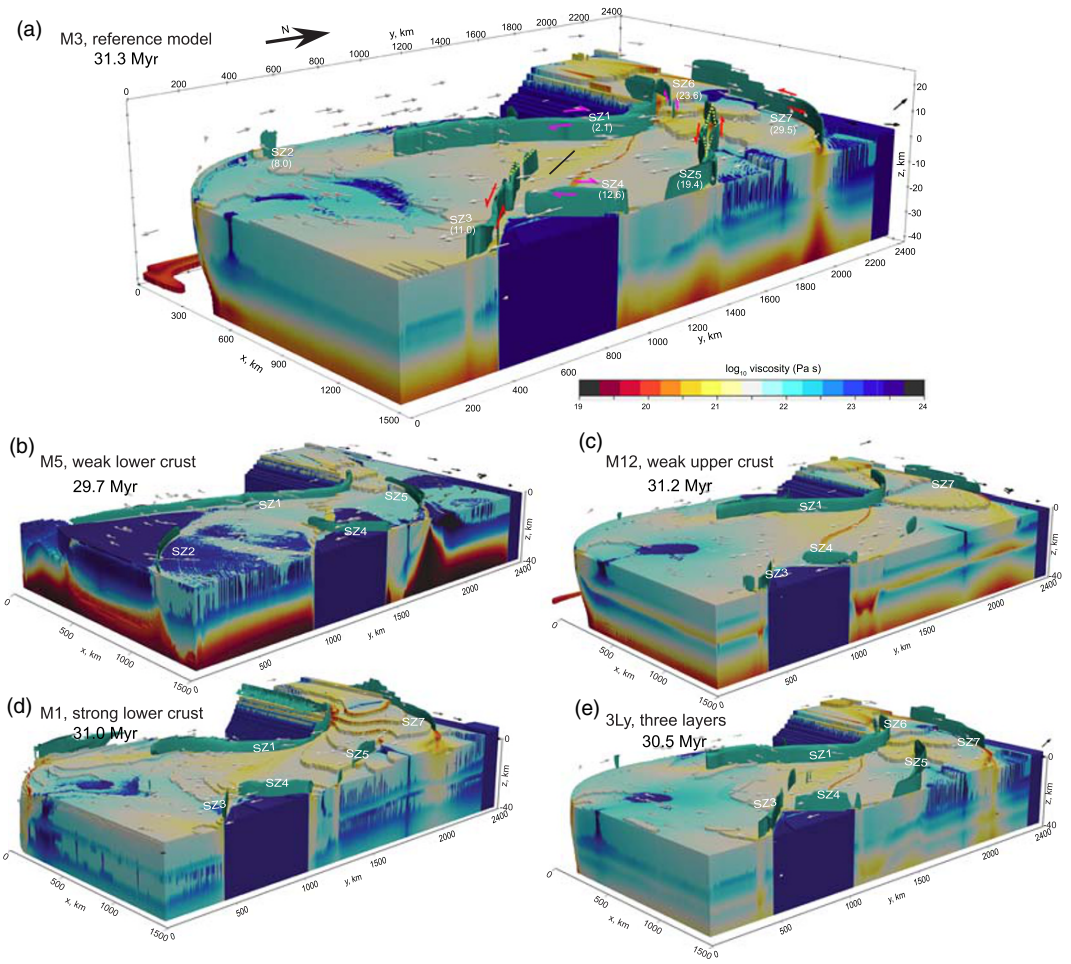

Figure 3. Visco-plastic viscosity of the reference model (a) and four comparative models (b–e). (a) Reference model (*M3*) uses $f_{uc} = 1$ and $f_{lc} = 1$ (see Figure 1c); (b) very weak lower crust (*M5*, $f_{lc} = 0.01$); (c) weak upper crust (*M12*, $f_{uc} = 0.01$); (d) strong lower crust (*M1*, $f_{lc} = 100$); and (e) three-layer crust (*3Ly*, $f_{mc} = 1$), respectively. The dark cyan contours are plastic strain (indicating faults/shear zones), white arrows indicate flow direction, and red and magenta arrows in (a) indicate left-lateral and right-lateral strike-slip faults (numbered shear zones SZ and their initiation time in Myr) cutting to the lower crust. Note that the vertical is exaggerated 10×, and the low viscosity zones that develop below the major brittle shear zones.

We assume Drucker-Prager yield criteria with which rocks fail plastically if the second invariant of the deviatoric stress ($\tau_{II} = \sqrt{0.5\tau_{ij}\tau_{ij}}$) exceed the yield stress τ_y (i.e., $\tau_{II} > \tau_y$). For Drucker-Prager non-associated plasticity this is expressed as

$$\tau_y = P\sin(\phi) + C\cos(\phi) \tag{3}$$

where P is the pressure, C is the cohesion, and ϕ is the effective friction angle. Plastic strain weakening of the friction angle is applied in the model which linearly decreases the friction angle from 30° to 3° between a strain of 0.5 and 1.5 (Table S1).

3. Results

We use a simplified tectonic geometry which includes the TB and three strong blocks in the north (SBN), the south (SBS, the Indian indenter), and the east (SBE), respectively (Figure 1). We focus on the formation of large-scale faults during continental collision, and the influence of crustal strength is discussed first, after

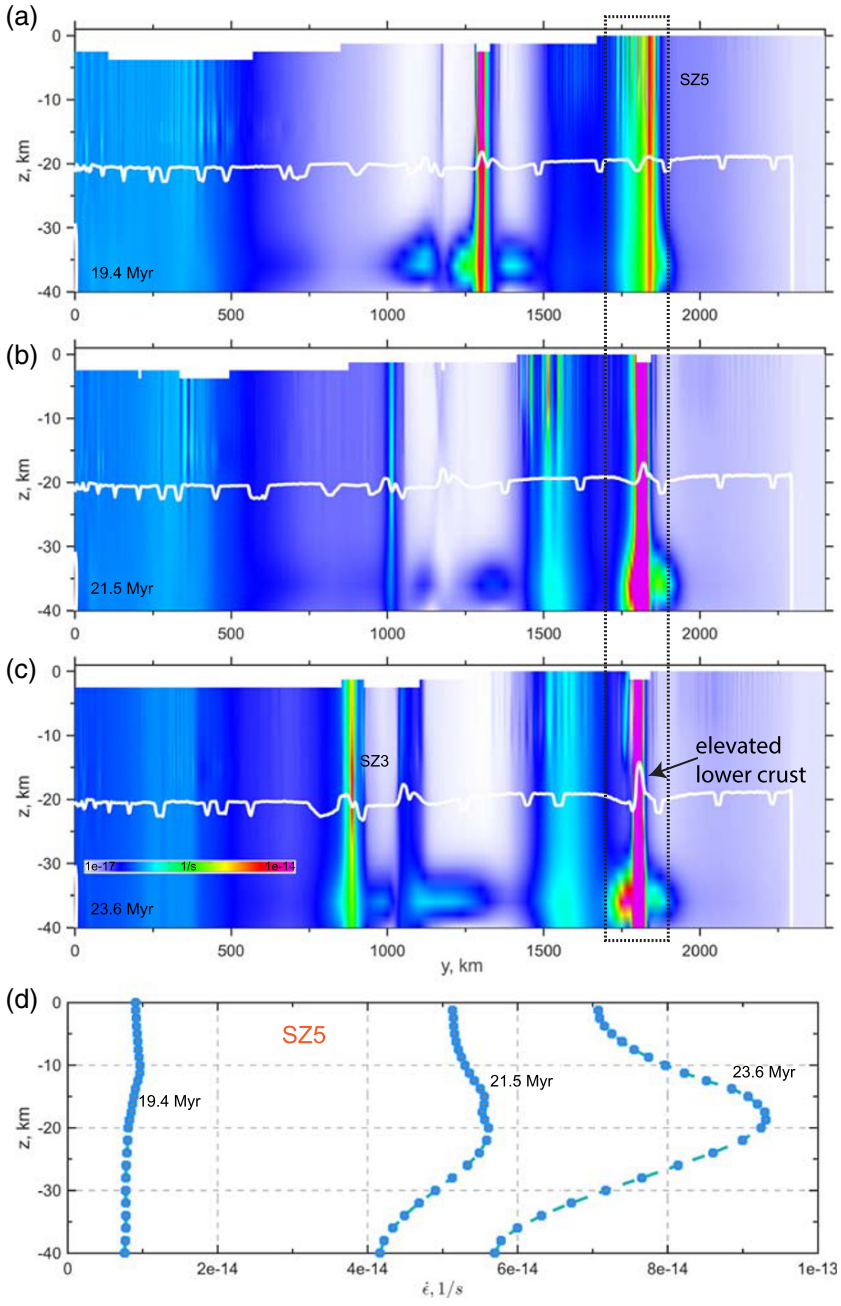

Figure 4. Development of a single shear zone. Second invariant strain rate $\dot{\varepsilon}_{II}$ profile along x = 1,200 km at time = 19.4 Myr (a), 21.5 Myr (b), and 23.6 Myr (c); the white lines are upper-lower crust boundary; (d) $\dot{\varepsilon}_{II}$ inside the shear zone in the vertical profile for SZ5 for the three snapshots.

which we present additional experiments to test the influence of shear heating and the location of the weak seeds. We start with explaining the reference model (*M3*) which best matches the observations.

3.1. Crustal Rheology Controls Strike-Slip Fault Formation

Upon the indentation of strong block SBS toward north (*y* direction), an intense simple shearing between the indenter and the adjacent TB block induces the first shear zone (or fault)—SZ1 (Figure 2). Six more shear zones successively develop within the TB block at later stages along either preset weak seeds or the boundary of strong blocks. The deformation is strongly concentrated along those narrow shear zones in the upper

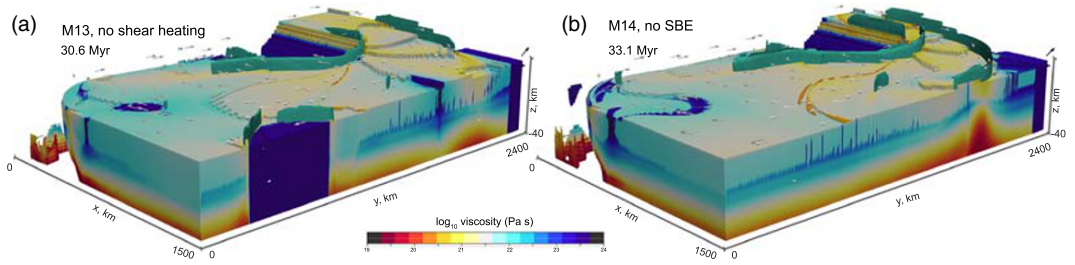

Figure 5. Two additional experiments compared to the reference Model *M3*: (a) Shear heating is deactivated. The dark cyan contours are plastic strain indicating faults/shear zones.

crust, while it is slightly more diffuse in the lower crust. The shear zones show a complex deformation pattern, exhibiting predominantly strike-slip motion, but also small amounts of thrust and/or normal slip within (e.g., SZ4, SZ5, and SZ7 in Figure 2). In front of the indenter, the lower crust is thickened and high topography develops, while the upper crust is extruded in east- and southeast-ward directions, rotating around a stationary point (Figure S1). Both thrust and normal faults occur in the frontal and side edges, respectively, due to compression and gravitational collapse. Escaping crust is blocked by SZ5, leading to thrust faulting in the northeast. When the indenter moves further northward, SZ5 rotates away from the indenter, extruded crustal material which is subsequently bounded by SZ7 formed along SBN. The shear zones are long, some being 1,000 km long, either continuous or segmented (Figure 3). They are either mostly left-lateral (SZ3, SZ5, and SZ7) or right-lateral (SZ1, SZ4, and SZ6). Slip displacements are large: SZ1 has offsets of ~100–400 km, SZ3 ~133 km, SZ5 ~382 km, and SZ7 ~378 km. There are also small widespread faults in the southeastern edge, primarily limited to the shallow upper crust at the early collision stage. In the southeast, no large shear zones develop within the crustal block between SZ1 and SZ3.

In order to test the impact of crustal strength on the dynamics, we perform four endmember simulations in which we test the effect of a very weak lower (*M5*; $f_{uc} = 1, f_{lc} = 0.01$, f being the scaling factor of viscosity in Equation 2) or a weak upper crust (*M12*; $f_{uc} = 0.01, f_{lc} = 1$), a strong lower crust (*M1*; $f_{uc} = 1, f_{lc} = 100$), and a case with a weak middle crust and a moderate lower crust (*3Ly*; $f_{mc} = 1$) (see Figure 3).

The simulation with a very weak lower crust (*M5*) shows a distinct behavior from others in that the upper crust is strongly thickened in front of the indenter, and the lower crust is almost exhumed to the surface beneath SZ5. SZ3 is not developed in Model *M5*, while SZ2, which is absent in the other models, is well developed. On the other hand, the case with a strong lower crust (*M1*) has far less remarkable shear zones, and a more pronounced thickening of the lower crust, which expands toward the east and southeast. Yet there is no correlation between the development of shear zones and thickening of the lower crust in Model *M1*. This also occurs for the case with a very weak upper crust (*M12*) in which shear zones are poorly developed, even though the lower crust undulation is similar as in Model *M3*. The case with a weak middle crust (*3Ly*) showed roughly similar shear zones as the reference simulation, but with less lower crustal elevation beneath the shear zones.

3.2. Initiation of Shear Zones

In the reference model, shear zones develop either along strength contrasts of two terranes or from local heterogeneities such as the initially imposed weak seeds. To have a better insight into the development of the shear zone, we describe SZ5 as an example (Figure 4). As a result of strike-slip motion, the lower crust moves upward and leads to ~6 km uplift of the lower crust, contemporaneously with the localization of SZ5. SZ5 initiates at ~12-km depth around 19 Myr and further localized at ~19 km. The whole crust is strongly deformed, resulting in a drastic undulation of the upper-lower crust interface, particularly in regions where shear localization occurs. The localization initiation depth can be either in the uppermost crust (<10 km) or in the middle crust (~15 km), but only those faults that are in the vicinity of large viscous terranes or that initiate from weak seeds extend to the lower crust depth and develop large-scale shear zones. This thus suggests that stress or mechanical heterogeneities play a key role in the initiation of such fault zones.

The model without shear heating (*M13*) exhibits less pronounced shear zones which generally locates around the strong terranes (Figure 5a). This points to a critical influence of shear heating (Kiss

et al., 2019; Leloup et al., 1999; Popov et al., 2012) and strong terranes on the strain localization. If we remove the strong block SBE (*M14* in Figure 5), SZ3 and SZ4 are not generated and SZ5 is very poorly developed. To test the influence of the weak seeds, four additional experiments are performed: We either remove the weak seed(s) or place it at a different position. The model results show that strike-slip faults still form without preset weak seeds, but they are shorter, as it is the case for SZ5 in the reference model, indicating a relatively weak correlation of the weak seed 1 with SZ5.

4. Discussion and Conclusions

Although the model geometry is simplified, these models are useful to understand the dynamics of crustal deformation during Himalayan-Tibetan orogeny. The nonlinear visco-elasto-plastic models show that an intermediate weak middle/lower crust (~10^{20} Pa·s) and a strong upper crust (>10^{22}Pa·s) can result in large-scale strike-slip faults which are roughly comparable to the ones observed in the Tibet region. For example, we suggest that SZ1 could correspond to the Sagaing Fault, SZ3 to the Xianshuihe Fault, SZ4 to the Longmenshan Fault, SZ5 to the Kunlun Fault, SZ6 to the Jiali Fault, and SZ7 to the Altyn-Tagh (or Haiyuan) Fault. Moreover, the deformation pattern in the upper crust shows the transition from barely deformed, less deformed, to deformed regions that are comparable with the northeast Tibet, the Songpan-Ganze, and the Chuandian fragments, respectively (Figure S1). A short indenter allows the crust to flow to the west after its passage, which results in an early developed SZ1 while the Sagaing Fault which might be affected by retreating Indian Plate was initiated at ~22–16 Ma (Searle et al., 2007, and reference therein). Interestingly, SZ2 that does not appear in the reference model, yet is developed when the lower crust is even weaker (<10^{19} Pa·s), indicating that the formation of Red River Fault is probably related to a locally weak crust. In contrast, deformation is less localized in the upper crust with no brittle faults if the upper crust is too weak. This implies that a seismogenic layer should be sufficiently strong. However, if the lower crust is too strong (>10^{22} Pa·s), the whole crust undergoes pure shear thickening which results in coherent deformation and less developed shear zones. Thus, the absent SZ2 may be potentially explained by different deformation styles due to along-strike rheological heterogeneities between the east-west (Bischoff & Flesch, 2019; Chen et al., 2017; Zheng et al., 2020) and the north-south (Huangfu et al., 2018) Tibetan terranes. Notably, the effective viscosities of upper and lower crust in our reference model are consistent with previous models which account for normal faulting and viscous buckling (Bischoff & Flesch, 2018; Flesch et al., 2001) in Tibet.

A comparison between Models *M3* and *M1* (*3Ly*) shows that a weak lower (middle) crust facilitates shear zone development (Figure 3). The locations of shear zones have a positive relationship with lower crust upwelling. The shear zones are usually localized at 15- to 20-km depth, with shear heating being the major heat source that lowers in situ strength and further promotes strain localization (Kaus & Podladchikov, 2006; Kiss et al., 2019; Leloup et al., 1999), while the initial thermal structure of the crust has a limited influence on the localization (Figures S2 and S3). The lower crust is uplifted beneath the shear zones, which is a robust feature in our simulations, further increasing the local temperature and facilitating strain localization. A similar increase in temperature and uplift of the middle crust has been documented in exhumed roots of large strike-slip faults (Leloup et al., 1999, and references therein). The uplift of the crustal flow probably indicates that the long-lived shear zones are predominantly transtensional (Le Pourhiet et al., 2014) or transpressional (Popov et al., 2012) during their formation. Our model results show that the shear zone close to a strong block likely exhibits reverse fault, transpression, and strike-slip fault; otherwise, it shows transtension and strike slip (Figure S4). Therefore, our model results predict a thickened lower crust with low seismic velocity beneath the major shear zones. This is consistent with seismic tomography and magnetotelluric observations of such low seismic velocity (Agius & Lebedev, 2014; Bao et al., 2015; Jiang et al., 2014; Liu et al., 2014; Wang et al., 2018) and high electrical conductivity zones (Bai et al., 2010; Wei et al., 2001) in the middle/lower crust beneath the Xianshuihe and Kunlun faults. Similar features have also locally been observed along the Altyn-Tagh Fault (Wittlinger et al., 1998; Zhang et al., 2015). Two remarkable seismic low-velocity channels (Figure 1) in southeast Tibet correlate with crustal thickening. It is worth noting that most large earthquakes occur within the boundaries of these two channels (Bao et al., 2015), which corroborates our finding that the formation of large-scale shear zones require/promote a weak and flowing middle/lower crust. Indeed, other numerical models also show that a weak middle to lower crust is required for the development of the N-S rifting systems in southern Tibet (Pang et al., 2018), as well as for the development of a wide plateau (Chen et al., 2017).

The reactivation of inherited weakness, such as ancient suture zones, is often proposed to control the location of lithosphere deformation during continental collision (Chen et al., 2020; Sun et al., 2018). However, few of the large-scale strike-slip faults in Asia geographically follow previous suture zones, with the notable exception of the Kunlun Fault (Tapponnier et al., 1986) (Figure 1). Previous models use weak zones that cannot sustain even small stresses (probably << few tens MPa) and thus localize deformation along the whole weak belt simultaneously, which is inconsistent with the observed diachronous initiation along strike-slip faults, such as Kunlun Fault which initiates in the west first and then propagates to the east (Duvall et al., 2013). In contrast, the presence of craton-like terranes in the periphery of Tibet, which sustains large stresses upon collision (Lu et al., 2011), does play a dominant role for the initiation of large-scale faults in our model (Figure 5b), consistent with geological observations in Tibet region.

The surface dynamics of continental extrusion during plate convergence is usually attributed to the mantle flow (Capitanio, 2014; Capitanio & Replumaz, 2013; Sternai et al., 2014). This would postulate that the mantle traction force is sufficiently large (Capitanio, 2020) and/or that the crust and mantle are coupled (Sol et al., 2007; Wang et al., 2008). However, our models show that a strong lower crust prohibits localized deformation, suggesting that the middle/lower crust is at least locally weak beneath the faults.

In conclusion, our simulations show that a moderately weak middle/lower crust is required to develop long-lived large-scale strike-slip faults as observed in Asia. The ongoing continental indentation pushes crustal blocks to "escape" toward northeast and southeast Tibet, causing tectonic forces and localized deformation along strike-slip faults that accommodate displacements. Deformation is primarily localized in shear zones which cut through the entire crust, whereas less pronounced deformation is localized in small faults in the rigid upper crust.

Data Availability Statement

The numerical source code used in this study is an open source online and also available from the link https://figshare.com/articles/LaMEM_TibetCollision/12571955, and the model setup to reproduce the results can be found on https://figshare.com/articles/inputdataTibet/12573236 or request from the corresponding author.

Acknowledgments

We acknowledge discussions with Adina Pusok, Tobias Baumann, comments by Xu Wang, and the computing time granted on the supercomputer MOGON II at Johannes Gutenberg University Mainz (hpc.uni-mainz.de) and TianHe-1(A) cluster at National Supercomputer Center in Tianjin (nscc-tj.cn). We also thank Lucy Flesch for editorial handling, Taras Gerya, and an anonymous reviewer for constructive review which greatly improved the presence of the paper. J. Y. was financially supported by China Scholarship Council. Y. L. was financially supported by CAS Pioneer Hundred Talents Program (Chinese Academy of Sciences). This research was supported by NSFC (Grants 41888101, 91755000, 41625016, and 41774112), National Key R&D Program of China (Grant 2017YFC0601206) and the Strategic Priority Research Program (B) of CAS (XDB18000000).

References

Agius, M. R., & Lebedev, S. (2014). Shear-velocity structure, radial anisotropy and dynamics of the Tibetan crust. *Geophysical Journal International*, *199*(3), 1395–1415. https://doi.org/10.1093/gji/ggu326

Bai, D., Unsworth, M. J., Meju, M. A., Ma, X., Teng, J., Kong, X., et al. (2010). Crustal deformation of the eastern Tibetan plateau revealed by magnetotelluric imaging. *Nature Geoscience*, *3*(5), 358–362. https://doi.org/10.1038/ngeo830

Bao, X., Sun, X., Xu, M., Eaton, D. W., Song, X., Wang, L., et al. (2015). Two crustal low-velocity channels beneath SE Tibet revealed by joint inversion of Rayleigh wave dispersion and receiver functions. *Earth and Planetary Science Letters*, *415*, 16–24. https://doi.org/10.1016/j.epsl.2015.01.020

Baumann, T., & Kaus, B. J. (2015). Geodynamic inversion to constrain the non-linear rheology of the lithosphere. *Geophysical Journal International*, *202*(2), 1289–1316. https://doi.org/10.1093/gji/ggv201

Bischoff, S., & Flesch, L. (2019). Impact of lithospheric strength distribution on India-Eurasia deformation from 3-D geodynamic models. *Journal of Geophysical Research: Solid Earth*, *124*, 1084–1105. https://doi.org/10.1029/2018JB015704

Bischoff, S. H., & Flesch, L. M. (2018). Normal faulting and viscous buckling in the Tibetan Plateau induced by a weak lower crust. *Nature Communications*, *9*, 4952. https://doi.org/10.1038/s41467-018-07312-9

Capitanio, F. A. (2014). The dynamics of extrusion tectonics: Insights from numerical modeling. *Tectonics*, *33*, 2361–2381. https://doi.org/10.1002/2014TC003688

Capitanio, F. A. (2020). Current deformation in the Tibetan Plateau: A stress gauge in the India-Asia collision tectonics. *Geochemistry, Geophysics, Geosystems*, *21*, e2019GC008649. https://doi.org/10.1029/2019GC008649

Capitanio, F. A., & Replumaz, A. (2013). Subduction and slab breakoff controls on Asian indentation tectonics and Himalayan western syntaxis formation. *Geochemistry, Geophysics, Geosystems*, *14*, 3515–3531. https://doi.org/10.1002/ggge.20171

Chen, L., Capitanio, F. A., Liu, L., & Gerya, T. V. (2017). Crustal rheology controls on the Tibetan plateau formation during India-Asia convergence. *Nature Communications*, *8*, 15992. https://doi.org/10.1038/ncomms15992

Chen, L., Liu, L., Capitanio, F. A., Gerya, T. V., & Li, Y. (2020). The role of pre-existing weak zones in the formation of the Himalaya and Tibetan plateau: 3-D thermomechanical modelling. *Geophysical Journal International*, *221*(3), 1971–1983. https://doi.org/10.1093/gji/ggaa125

Clark, M. K., & Royden, L. H. (2000). Topographic ooze: Building the eastern margin of Tibet by lower crustal flow. *Geology*, *28*(8), 703–706. https://doi.org/10.1130/0091-7613(2000)28<703:TOBTEM>2.0.CO;2

Copley, A., Avouac, J.-P., & Wernicke, B. P. (2011). Evidence for mechanical coupling and strong Indian lower crust beneath southern Tibet. *Nature*, *472*(7341), 79–81. https://doi.org/10.1038/nature09926

Crameri, F., Schmeling, H., Golabek, G., Duretz, T., Orendt, R., Buiter, S., et al. (2012). A comparison of numerical surface topography calculations in geodynamic modelling: An evaluation of the 'sticky air' method. *Geophysical Journal International*, *189*(1), 38–54. https://doi.org/10.1111/j.1365-246X.2012.05388.x

Dong, H., Wei, W., Jin, S., Ye, G., Zhang, L., Jing, J. E., et al. (2016). Extensional extrusion: Insights into south-eastward expansion of Tibetan Plateau from magnetotelluric array data. *Earth and Planetary Science Letters*, *454*, 78–85. https://doi.org/10.1016/j.epsl.2016.07.043

Duretz, T., de Borst, R., Yamato, P., & Le Pourhiet, L. (2020). Toward robust and predictive geodynamic modeling: The way forward in frictional plasticity. *Geophysical Research Letters*, *47*, e2019GL086027. https://doi.org/10.1029/2019GL086027

Duvall, A. R., Clark, M. K., Kirby, E., Farley, K. A., Craddock, W. H., Li, C., & Yuan, D. Y. (2013). Low-temperature thermochronometry along the Kunlun and Haiyuan Faults, NE Tibetan Plateau: Evidence for kinematic change during late-stage orogenesis. *Tectonics*, *32*, 1190–1211. https://doi.org/10.1002/tect.20072

England, P., & McKenzie, D. (1982). A thin viscous sheet model for continental deformation. *Geophysical Journal International*, *70*(2), 295–321. https://doi.org/10.1111/j.1365-246X.1982.tb04969.x

Flesch, L. M., Haines, A. J., & Holt, W. E. (2001). Dynamics of the India-Eurasia collision zone. *Journal of Geophysical Research*, *106*(B8), 16,435–16,460. https://doi.org/10.1029/2001JB000208

Gan, W. J., Zhang, P. Z., Shen, Z. K., Niu, Z. J., Wang, M., Wan, Y. G., et al. (2007). Present-day crustal motion within the Tibetan Plateau inferred from GPS measurements. *Journal of Geophysical Research*, *112*, B08416. https://doi.org/10.1029/2005JB004120

Houseman, G., & England, P. (1986). Finite strain calculations of continental deformation: 1. Method and general results for convergent zones. *Journal of Geophysical Research*, *91*(B3), 3651–3663. https://doi.org/10.1029/JB091iB03p03651

Huangfu, P., Li, Z.-H., Gerya, T., Fan, W., Zhang, K.-J., Zhang, H., & Shi, Y. (2018). Multi-terrane structure controls the contrasting lithospheric evolution beneath the western and central–eastern Tibetan plateau. *Nature Communications*, *9*, 3780. https://doi.org/10.1038/s41467-018-06233-x

Jiang, C., Yang, Y., & Zheng, Y. (2014). Penetration of mid-crustal low velocity zone across the Kunlun Fault in the NE Tibetan Plateau revealed by ambient noise tomography. *Earth and Planetary Science Letters*, *406*, 81–92. https://doi.org/10.1016/j.epsl.2014.08.040

Kaus, B. J. (2016). Constraining lithospheric flow. *Science*, *353*(6307), 1495–1496. https://doi.org/10.1126/science.aai8442

Kaus, B. J., Mühlhaus, H., & May, D. A. (2010). A stabilization algorithm for geodynamic numerical simulations with a free surface. *Physics of the Earth and Planetary Interiors*, *181*(1–2), 12–20. https://doi.org/10.1016/j.pepi.2010.04.007

Kaus, B. J. P., & Podladchikov, Y. Y. (2006). Initiation of localized shear zones in viscoelastoplastic rocks. *Journal of Geophysical Research*, *111*, B04412. https://doi.org/10.1029/2005JB003652

Kaus, B. J. P., Popov, A. A., Baumann, T., Pusok, A. E., Bauvile, A., Fernandez, N., & Collignon, M. (2016). *Forward and inverse modelling of lithospheric deformation on geological timescales*. Paper presented at Proceedings of NIC Symposium.

Kiss, D., Podladchikov, Y., Duretz, T., & Schmalholz, S. M. (2019). Spontaneous generation of ductile shear zones by thermal softening: Localization criterion, 1D to 3D modelling and application to the lithosphere. *Earth and Planetary Science Letters*, *519*, 284–296. https://doi.org/10.1016/j.epsl.2019.05.026

Le Pape, F., Jones, A. G., Vozar, J., & Wenbo, W. (2012). Penetration of crustal melt beyond the Kunlun Fault into northern Tibet. *Nature Geoscience*, *5*(5), 330–335. https://doi.org/10.1038/ngeo1449

Le Pourhiet, L., Huet, B., & Traoré, N. (2014). Links between long-term and short-term rheology of the lithosphere: Insights from strike-slip fault modelling. *Tectonophysics*, *631*, 146–159. https://doi.org/10.1016/j.tecto.2014.06.034

Lechmann, S. M., May, D. A., Kaus, B. J. P., & Schmalholz, S. M. (2011). Comparing thin-sheet models with 3-D multilayer models for continental collision. *Geophysical Journal International*, *187*(1), 10–33. https://doi.org/10.1111/j.1365-246X.2011.05164.x

Leloup, P. H., Ricard, Y., Battaglia, J., & Lacassin, R. (1999). Shear heating in continental strike-slip shear zones: Model and field examples. *Geophysical Journal International*, *136*(1), 19–40. https://doi.org/10.1046/j.1365-246X.1999.00683.x

Li, H., Shen, Y., Huang, Z., Li, X., Gong, M., Shi, D., et al. (2014). The distribution of the mid-to-lower crustal low-velocity zone beneath the northeastern Tibetan Plateau revealed from ambient noise tomography. *Journal of Geophysical Research: Solid Earth*, *119*, 1954–1970. https://doi.org/10.1002/2013JB010374

Li, X., Ma, X., Chen, Y., Xue, S., Varentsov, I. M., & Bai, D. (2020). A plume-modified lithospheric barrier to the southeastward flow of partially molten Tibetan crust inferred from magnetotelluric data. *Earth and Planetary Science Letters*, *548*, 116493. https://doi.org/10.1016/j.epsl.2020.116493

Li, Y., Liu, M., Wang, Q., & Cui, D. (2018). Present-day crustal deformation and strain transfer in northeastern Tibetan Plateau. *Earth and Planetary Science Letters*, *487*, 179–189. https://doi.org/10.1016/j.epsl.2018.01.024

Li, Z.-H., Xu, Z., Gerya, T., & Burg, J.-P. (2013). Collision of continental corner from 3-D numerical modeling. *Earth and Planetary Science Letters*, *380*, 98–111. https://doi.org/10.1016/j.epsl.2013.08.034

Liu, L., & Hasterok, D. (2016). High-resolution lithosphere viscosity and dynamics revealed by magnetotelluric imaging. *Science*, *353*(6307), 1515–1519. https://doi.org/10.1126/science.aaf6542

Liu, Q. Y., van der Hilst, R. D., Li, Y., Yao, H. J., Chen, J. H., Guo, B., et al. (2014). Eastward expansion of the Tibetan Plateau by crustal flow and strain partitioning across faults. *Nature Geoscience*, *7*(5), 361–365. https://doi.org/10.1038/ngeo2130

Lu, G., Kaus, B. J., & Zhao, L. (2011). Thermal localization as a potential mechanism to rift cratons. *Physics of the Earth and Planetary Interiors*, *186*(3-4), 125–137. https://doi.org/10.1016/j.pepi.2011.04.006

Lu, G., Zhao, L., Zheng, T., Wang, K., & Yang, J. (2016). Determining the key conditions for the formation of metamorphic core complexes by geodynamic modeling and insights into the destruction of North China Craton. *Science China Earth Sciences*, *59*(9), 1873–1884. https://doi.org/10.1007/s11430-015-5407-5

Molnar, P., & Tapponnier, P. (1975). Cenozoic tectonics of Asia: Effects of a continental collision. *Science*, *189*(4201), 419–426. https://doi.org/10.1126/science.189.4201.419

Nelson, K. D., Zhao, W., Brown, L., Kuo, J., Che, J., Liu, X., et al. (1996). Partially molten middle crust beneath southern Tibet: Synthesis of project INDEPTH results. *Science*, *274*(5293), 1684–1688. https://doi.org/10.1126/science.274.5293.1684

Pang, Y., Zhang, H., Gerya, T. V., Liao, J., Cheng, H., & Shi, Y. (2018). The mechanism and dynamics of N-S rifting in southern Tibet: Insight from 3-D thermomechanical modeling. *Journal of Geophysical Research: Solid Earth*, *123*, 859–877. https://doi.org/10.1002/2017JB014011

Popov, A. A., Sobolev, S. V., & Zoback, M. D. (2012). Modeling evolution of the San Andreas Fault system in northern and central California. *Geochemistry, Geophysics, Geosystems*, *13*, Q08016. https://doi.org/10.1029/2012GC004086

Pusok, A., & Kaus, B. J. (2015). Development of topography in 3-D continental-collision models. *Geochemistry, Geophysics, Geosystems*, *16*, 1378–1400. https://doi.org/10.1002/2015GC005732

Pusok, A. E., Kaus, B. J., & Popov, A. A. (2017). On the quality of velocity interpolation schemes for marker-in-cell method and staggered grids. *Pure and Applied Geophysics*, *174*(3), 1071–1089. https://doi.org/10.1007/s00024-016-1431-8

Pusok, A. E., Kaus, B. J. P., & Popov, A. A. (2018). The effect of rheological approximations in 3-D numerical simulations of subduction and collision. *Tectonophysics*, *746*, 296–311. https://doi.org/10.1016/j.tecto.2018.04.017

Replumaz, A., Funiciello, F., Reitano, R., Faccenna, C., & Balon, M. (2016). Asian collisional subduction: A key process driving formation of the Tibetan Plateau. *Geology*, *44*(11), 943–946. https://doi.org/10.1130/G38276.1

Replumaz, A., & Tapponnier, P. (2003). Reconstruction of the deformed collision zone between India and Asia by backward motion of lithospheric blocks. *Journal of Geophysical Research*, *108*(B6), 2285. https://doi.org/10.1029/2001JB000661

Royden, L. H., Burchfiel, B. C., King, R. W., Wang, E., Chen, Z., Shen, F., & Liu, Y. (1997). Surface deformation and lower crustal flow in eastern Tibet. *Science*, *276*(5313), 788–790. https://doi.org/10.1126/science.276.5313.788

Searle, M. P., Noble, S. R., Cottle, J. M., Waters, D. J., Mitchell, A. H. G., Hlaing, T., & Horstwood, M. S. A. (2007). Tectonic evolution of the Mogok metamorphic belt, Burma (Myanmar) constrained by U-Th-Pb dating of metamorphic and magmatic rocks. *Tectonics*, *26*, 158. https://doi.org/10.1029/2006tc002083

Sol, S., Meltzer, A., Bürgmann, R., Van der Hilst, R., King, R., Chen, Z., et al. (2007). Geodynamics of the southeastern Tibetan Plateau from seismic anisotropy and geodesy. *Geology*, *35*(6), 563–566. https://doi.org/10.1130/G23408A.1

Sternai, P., Jolivet, L., Menant, A., & Gerya, T. (2014). Driving the upper plate surface deformation by slab rollback and mantle flow. *Earth and Planetary Science Letters*, *405*, 110–118. https://doi.org/10.1016/j.epsl.2014.08.023

Sun, M., Yin, A., Yan, D., Ren, H., Mu, H., Zhu, L., & Qiu, L. (2018). Role of pre-existing structures in controlling the Cenozoic tectonic evolution of the eastern Tibetan plateau: New insights from analogue experiments. *Earth and Planetary Science Letters*, *491*, 207–215. https://doi.org/10.1016/j.epsl.2018.03.005

Tapponnier, P., Peltzer, G., & Armijo, R. (1986). On the mechanics of the collision between India and Asia. *Geological Society, London, Special Publications*, *19*(1), 113–157. https://doi.org/10.1144/GSL.SP.1986.019.01.07

Tapponnier, P., Peltzer, G., Le Dain, A., Armijo, R., & Cobbold, P. (1982). Propagating extrusion tectonics in Asia: New insights from simple experiments with plasticine. *Geology*, *10*(12), 611–616. https://doi.org/10.1130/0091-7613(1982)10<611:PETIAN>2.0.CO;2

Tapponnier, P., Zhiqin, X., Roger, F., Meyer, B., Arnaud, N., Wittlinger, G., & Jingsui, Y. (2001). Oblique stepwise rise and growth of the Tibet Plateau. *Science*, *294*(5547), 1671–1677. https://doi.org/10.1126/science.105978

Wang, C. Y., Flesch, L. M., Silver, P. G., Chang, L. J., & Chan, W. W. (2008). Evidence for mechanically coupled lithosphere in central Asia and resulting implications. *Geology*, *36*(5), 363–366. https://doi.org/10.1130/G24450A.1

Wang, X., Chen, L., Ai, Y., Xu, T., Jiang, M., Ling, Y., & Gao, Y. (2018). Crustal structure and deformation beneath eastern and northeastern Tibet revealed by P-wave receiver functions. *Earth and Planetary Science Letters*, *497*, 69–79. https://doi.org/10.1016/j.epsl.2018.06.007

Wang, X., Kaus, B. J. P., Zhao, L., Yang, J., & Li, Y. (2019). Mountain building in Taiwan: Insights from 3-D geodynamic models. *Journal of Geophysical Research: Solid Earth*, *124*, 5924–5950. https://doi.org/10.1029/2018JB017165

Wei, W., Le Pape, F., Jones, A. G., Vozar, J., Dong, H., Unsworth, M. J., et al. (2014). Northward channel flow in northern Tibet revealed from 3D magnetotelluric modelling. *Physics of the Earth and Planetary Interiors*, *235*, 13–24. https://doi.org/10.1016/j.pepi.2014.07.004

Wei, W., Unsworth, M., Jones, A., Booker, J., Tan, H., Nelson, D., et al. (2001). Detection of widespread fluids in the Tibetan crust by magnetotelluric studies. *Science*, *292*(5517), 716–719. https://doi.org/10.1126/science.1010580

Wittlinger, G., Tapponnier, P., Poupinet, G., Mei, J., Danian, S., Herquel, G., & Masson, F. (1998). Tomographic evidence for localized lithospheric shear along the Altyn Tagh fault. *Science*, *282*(5386), 74–76. https://doi.org/10.1126/science.282.5386.74

Wu, C., Tian, X., Xu, T., Liang, X., Chen, Y., Zhu, G., et al. (2019). Upper-crustal anisotropy of the conjugate strike-slip fault zone in central Tibet analyzed using local earthquakes and shear-wave splitting. *Bulletin of the Seismological Society of America*, *109*(5), 1968–1984. https://doi.org/10.1785/0120180333

Yin, A., & Harrison, T. M. (2000). Geologic evolution of the Himalayan-Tibetan orogen. *Annual Review of Earth and Planetary Sciences*, *28*(1), 211–280. https://doi.org/10.1146/annurev.earth.28.1.211

Zhang, L., Unsworth, M., Jin, S., Wei, W., Ye, G., Jones, A. G., et al. (2015). Structure of the Central Altyn Tagh Fault revealed by magnetotelluric data: New insights into the structure of the northern margin of the India–Asia collision. *Earth and Planetary Science Letters*, *415*, 67–79. https://doi.org/10.1016/j.epsl.2015.01.025

Zheng, T., He, Y., Ding, L., Jiang, M., Ai, Y., Mon, C. T., et al. (2020). Direct structural evidence of Indian continental subduction beneath Myanmar. *Nature Communications*, *11*, 1944. https://doi.org/10.1038/s41467-020-15746-3